Hexagonal $Na_{1.5}Y_{1.5}F_6$ at High Pressures

A. Grzechnik,*,[1] P. Bouvier,† M. Mezouar,† M. D. Mathews,‡ A. K. Tyagi,‡ and J. Köhler*

*Max-Planck-Institut für Festkörperforschung, Heisenbergstr. 1, D-70569 Stuttgart, Germany; †European Synchrotron Radiation Facility, B.P. 220, F-38000 Grenoble, France; and ‡Applied Chemistry Division, Bhabha Atomic Research Centre, Trombay, Mumbai 400 085, India
E-mail: andrzej@servix.mpi-stuttgart.mpg.de

The high-pressure behavior of hexagonal $Na_{1.5}Y_{1.5}F_6$ is investigated with synchrotron angle-dispersive X-ray powder diffraction in a diamond anvil cell up to 22 GPa at room temperature. There is no major phase transition in this material in the entire pressure region studied here. At near ambient pressures, the structure is of the $Na_{1.5}Nd_{1.5}F_6$ type ($P\bar{6}$, $Z = 1$), found in other low-temperature sodium lanthanide fluorides. Pressure-induced order–disorder phenomena lead to the formation of the gagarinite structure ($P6_3/m$, $Z = 1$) above 20 GPa. Alternatively, the pressure-induced order–disorder phenomena could be related to a polymorphic transition towards the phase of the β-Na_2ThF_6 type with $P\bar{6}2m$ ($Z = 1$) symmetry. There is no volume change associated with all these reversible structural changes. © 2002 Elsevier Science (USA)

INTRODUCTION

Fluorides have attracted interest as laser materials because of their lower phonon energies when compared to oxides, resistance to short wavelength radiation, relatively high optical damage threshold, and low non-linear refractive indices (1, 2). Their large gaps and low phonon energies result in lower multiphonon emission rates and high luminescence efficiencies. $LiYF_4$ is already a commercially used host material for laser systems. Recent studies of up-conversion processes of IR photons to blue emission in doped hexagonal $Na_{1.5}Ln_{1.5}F_6$ (Ln = La–Tm, Y) powder samples suggest that they could serve as diode-pumped IR solid-state lasers or be useful for up-conversion laser action (2). In addition, rare-earth-doped $Na_{1.5}Y_{1.5}F_6$ exhibits a photoluminescence output comparable to the $LiYF_4$ phosphor (3).

The wavelength of the emission is influenced by the crystal field, which causes a splitting of the energy levels. The richest variety of laser wavelengths is found in rare-earth-doped fluoride compounds featuring ordered structures (1).

The high efficiency of the luminescence mechanism in $Na_{1.5}Y_{1.5}F_6$ is due to a multisite character of its crystal lattice (2, 3). Therefore, in order to better understand the chemical bonding and interactions between central ions and their crystalline environment in this and other fluorides, further studies at various pressure–temperature conditions are required. $LiYF_4$ has already been a subject of investigations on lattice dynamics (4) as well as Raman scattering (5), luminescence (6), and X-ray powder diffraction (7) at high pressures. There is no such information available on any of the $Na_{1.5}Ln_{1.5}F_6$ compounds. Since their luminescent properties mainly depend on ordering of the cations and their crystalline surrounding, a detailed study of the crystal structure as a function of pressure and/or temperature would provide useful information for crystal field considerations. Here, we investigate a high-pressure room-temperature behavior of hexagonal $Na_{1.5}Y_{1.5}F_6$ with angle-dispersive X-ray powder diffraction in a diamond anvil cell.

EXPERIMENTAL

NaF (Alfa, 99.9%) and YF_3 (Alfa, 99.9%), used as the starting materials, were dried in a dynamic vacuum (10^{-5} Torr) at 300°C prior to further use. A mechanical mixture of NaF and YF_3 was prepared in a 1:1 molar ratio and pressed into a pellet kept in an argon-filled platinum tube. The tube was then placed in an argon-filled quartz glass ampoule. The ampoule was slowly heated to 930°C and held there for 24 h, followed by a slow cooling to room temperature. The X-ray powder data were collected using $CuK\alpha_1$ radiation, monochromatized by a curved germanium crystal (111) face, on a Stoe-STADI diffractometer equipped with a PSD detector. The obtained pattern, in which an impurity of $NaYF_4$ fluorite ($Fm\bar{3}m$) was detected (about 1 wt%), can be indexed (8) on the basis of a hexagonal unit cell with $a = 5.9726(6)$ Å, $c = 3.5282(6)$ Å, and $V = 108.99(4)$ Å^3 and with no extinction rules [$M(20) = 87.8$, $F(20) = 52.7$].

The powder sample was loaded into a diamond anvil cell with a nitrogen pressure medium. Angle-dispersive powder

X-ray diffractograms at high pressures and room temperature were measured on the ID30 beamline at the European Synchrotron Radiation Facility, Grenoble. Monochromatic radiation at a wavelength of 0.3738(1) Å was used for pattern collection on image plates. The images were integrated using the program FIT2D (9) to yield intensity versus 2θ diagrams. The ruby luminescence method (10) was used for pressure calibration.

Full Rietveld refinements of the X-ray patterns were carried out using the program GSAS (11). The refined parameters were: the fractional coordinates, isotropic thermal parameters, Chebyshev polynomial background, Stephens profile function (12), an overall intensity scaling factor, zero shift, and cell parameters. Fractional and split occupancies as well as a preferred orientation correction were not refined. Bragg reflections from the solid phases of nitrogen (13) were subtracted from the patterns prior to the refinements.

STRUCTURAL MODELS

Lanthanide tetrafluorides of sodium and potassium at atmospheric pressure are derivatives of the CaF_2 fluorite type ($Fm\bar{3}m$, $Z = 4$). The ideal cubic structure is present in $NaLnF_4$ ($Ln = $ Ho–Lu, Y) (14–16) and $KLnF_4$ ($Ln = $ La, Ce) (17), while the compounds $KLnF_4$ ($Ln = $ Gd–Lu, Y) (18) have a trigonal superstructure ($P3_1$, $Z = 18$). $KCeF_4$ is dimorphous with α cubic and β orthorhombic ($Pnma$, $Z = 4$) phases (19). Low-temperature structures of the compounds containing sodium are hexagonal with a general formula $Na_{1.5}Ln_{1.5}F_6$ ($Ln = $ La–Tm, Y). For the series with $Ln = $ La, Ce, Pr, Nd, Eu, Gd, Tb, Ho, and Er the space group is $P\bar{6}$ ($Z = 1$), while it is supposed to be $P6_3/m$ ($Z = 1$) for $Ln = $ Y, Sm, and Tm (20).

There are three types of cationic sites in the structural model for $Na_{1.5}Ln_{1.5}F_6$ with $P\bar{6}$ symmetry (20): a nine-fold coordinated position occupied by Ln^{3+} (site 1a), another nine-fold coordinated position occupied randomly by $\frac{1}{2}Na^+$ and $\frac{1}{2}Ln^{3+}$ (site 1f), and a six-fold coordinated one occupied by $\frac{1}{2}Na^+$ and vacancies (site 2h) (Fig. 1). The polyhedra about the first two positions are tricapped trigonal prisms, and about the third one are irregular octahedra. This structure becomes the same as that of the other compounds with space group $P6_3/m$ (the gagarinite $NaCaLnF_6$ type) when the cations of the first two sites are entirely intermixed (20, 21). As a result, the coordination polyhedra around the ($\frac{3}{4}Ln^{3+}$, $\frac{1}{4}Na^+$) position are tricapped trigonal prisms (site 2d), while the remaining sodium ions are split between partially occupied positions with tricapped trigonal prism and trigonal antiprism coordinations (two sites 4e) (21). Recent reports on Eu^{3+} and Pr^{3+} luminescence, serving as a probe for site symmetry, have confirmed the structural model in space group $P\bar{6}$ for all of the $Na_{1.5}Ln_{1.5}F_6$ compounds, including $Na_{1.5}Y_{1.5}F_6$, at room and low
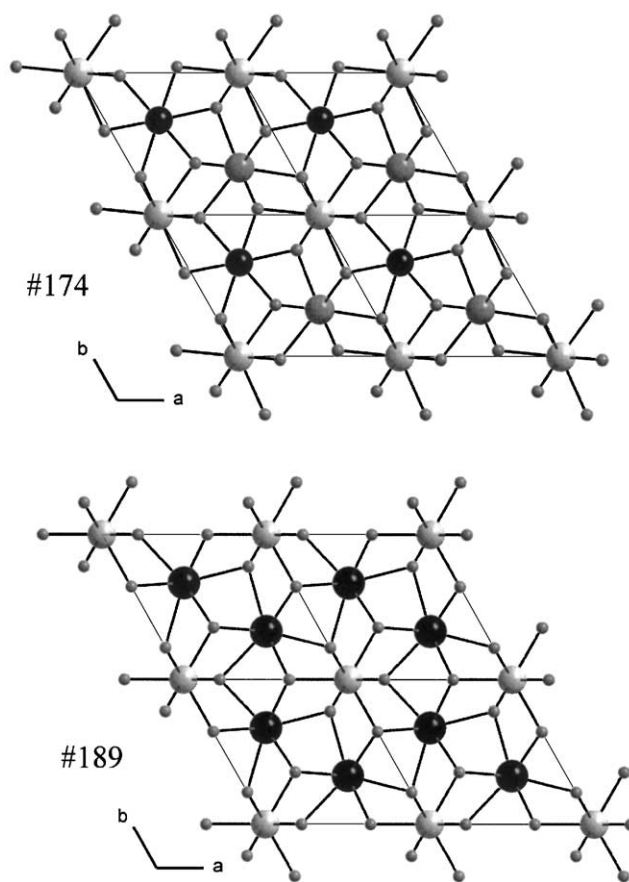
FIG. 1. Crystal structures of $Na_{1.5}Y_{1.5}F_6$ with $P\bar{6}$ (#174) and $P\bar{6}2m$ (#189) symmetries in the projection on the (a, b) plane. The small gray symbols are fluorine atoms. In the #174 structure, the large black, medium gray, and light gray symbols stand for the $\frac{1}{2}Na^+$, ($\frac{1}{2}Na^+$, $\frac{1}{2}Y^{3+}$), and Y^{3+} sites, respectively. The large back and light gray symbols in the #189 projection represent the ($\frac{3}{4}Na^+$, $\frac{1}{4}Y^{3+}$) and Y^{3+} positions, respectively.

temperatures (2, 3, 22). The gagarinite–fluorite $P6_3/m \rightarrow Fm\bar{3}m$ phase transition occuring at high temperature is of the order–disorder character with respect to the cations (21). This transformation results in a random distribution of all the cations over one crystallographic position in the fluorite structure ($Fm\bar{3}m$). It is worth noting that β-$KCeF_4$ ($Pnma$, $Z = 4$) has a gagarinite-type superstructure (23, 24).

Related to the gagarinite-like types is the structure of β-Na_2ThF_6 and β_1-K_2UF_6 ($P\bar{6}2m$, $Z = 1$) (25, 26) proposed for $K_{1.5}La_{1.5}F_6$ and $K_{1.5}Ce_{1.5}F_6$ (25). In fact, the structure of hexagonal $Na_{1.5}Y_{1.5}F_6$ was initially assigned to this type (14). Zachariasen's structure (25) is very similar to the $P\bar{6}$ one (20) (Fig. 1), the main difference being the absence of the octahedral $\frac{1}{2}Na^+$ positions. Two available cationic positions at the sites 2d and 1a have a nine-fold coordination and the ions are distributed as ($\frac{3}{4}Na^+$, $\frac{1}{4}Ln^{3+}$) and Ln^{3+}, respectively. In the projection on the (a, b) plane, the ($\frac{1}{2}Na^+$, $\frac{1}{2}Ln^{3+}$) and $\frac{1}{2}Na^+$ positions in the $P\bar{6}$ symmetry are no

longer distinguishable in space group $P\bar{6}2m$. The structure of KPbLaF$_6$ gagarinite has also been given with $P\bar{6}2m$ symmetry by Dib *et al.* (24).

RESULTS AND DISCUSSION

Powder X-ray diffraction patterns of Na$_{1.5}$Y$_{1.5}$F$_6$ as a function of pressure are shown in Fig. 2. There is no indication for any major structural transformation in this compound up to about 22 GPa. The most important observation is that the 001 peak vanishes above 20 GPa. In fact, the intensity of the 00l reflections is used to distinguish between the space groups with no selection rules, i.e., $P\bar{6}$ and $P\bar{6}2m$, and space group $P6_3/m$ ($l = 2n$). It was already pointed out by Burns (20) and Frank-Kamenetskaya *et al.*
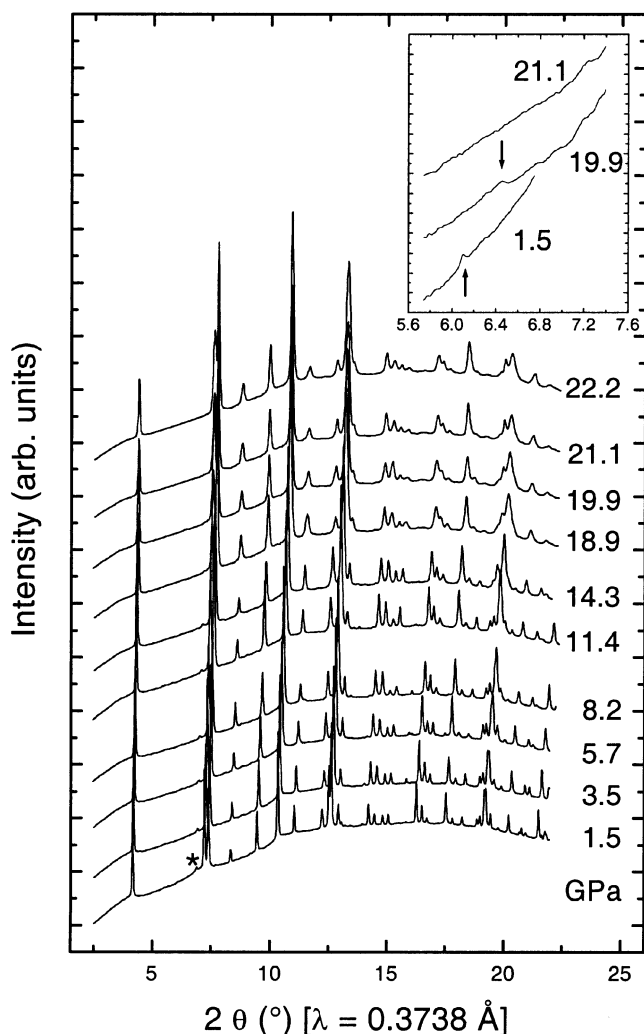
FIG. 2. Selected X-ray powder diffraction patterns of Na$_{1.5}$Y$_{1.5}$F$_6$. The numbers indicate pressures in GPa. The star marks the (111) reflection of NaYF$_4$ fluorite ($Fm\bar{3}m$). In the inset the pressure evolution of the (001) reflection (marked with arrows) in hexagonal Na$_{1.5}$Y$_{1.5}$F$_6$ is shown. Bragg reflections due to solid phases of nitrogen (13) are subtracted.
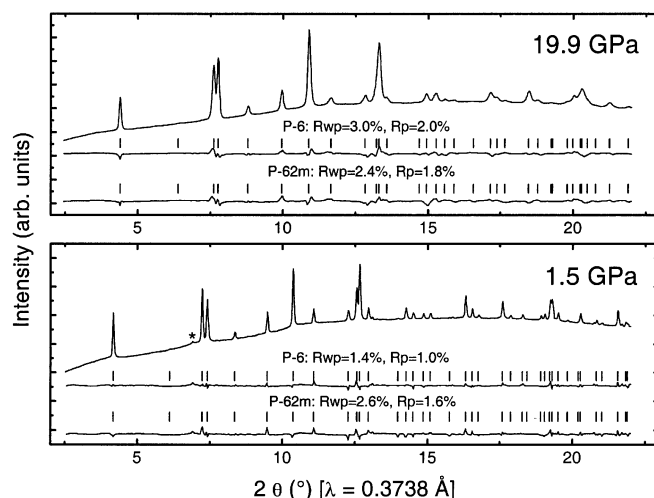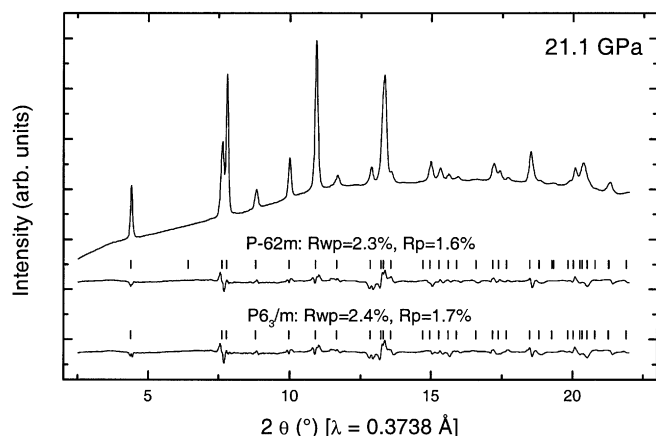

FIG. 3. Results of full profile Rietveld refinements of the patterns collected at 1.5 and 19.9 GPa. Each diagram was refined with two structural models in space groups $P\bar{6}$ and $P\bar{6}2m$. The top and bottom sets of symbols, ticks (marking the positions of Bragg reflections), and difference curves are for the $P\bar{6}$ and $P\bar{6}2m$ models, respectively. The residuals Rwp and Rp, whose definitions are given in the GSAS manual (11), are calculated only for the Bragg contribution to the diffraction patterns. Bragg reflections due to the solid $R\bar{3}c$ phase of nitrogen (13) are subtracted.

(21) that the 00l intensities depend on the distribution of cations at the 1a and 1f sites of space group $P\bar{6}$. If these cations are randomly distributed, the 00l peaks with the extinction $l = 2n$ are only observed and the symmetry of the crystal lattice is $P6_3/m$.

To gain more insight into the distribution of the cations and the possible symmetry changes, we used the Rietveld method (11) to refine selected diagrams with different structural models (Figs. 3 and 4, Tables 1–6). At pressures below 20 GPa, each diagram was refined with two structure types in space groups $P\bar{6}$ and $P\bar{6}2m$. The starting positional parameters for the atoms were those for Na$_{1.5}$Nd$_{1.5}$F$_6$ (20) and K$_{1.5}$Ce$_{1.5}$F$_6$ (25), respectively. The structure in $P\bar{6}2m$ has only two available nine-fold coordinated cationic positions, with no distortion of the anionic sublattice (Fig. 1). Based on small differences in Rwp and Rp residuals, the $P\bar{6}$ model would be preferable at relatively low pressures (Fig. 3, Tables 1 and 2). It is in agreement with recent reports on Ln^{3+} luminescence in hexagonal Na$_{1.5}$Y$_{1.5}$F$_6$ that clearly demonstrated the existence of three luminescent sites present in the $P\bar{6}$ polymorph at ambient conditions (2, 3, 22), while only two cationic sites are available for lanthanide doping in the $P\bar{6}2m$ structure (25). On the other hand, the residuals for the $P\bar{6}2m$ structure are slightly smaller at higher pressures. Zachariasen's $P\bar{6}2m$ model (25) differs from the one of the $P\bar{6}$ type by a higher disorder in cation distribution.

For the refinement of the diagrams, at which the 00l reflections are no longer observed (Fig. 4), we used the

FIG. 4. Results of full profile Rietveld refinements of the pattern collected at 21.1 GPa. The diagram was refined with two structural models in space groups $P\bar{6}2m$ and $P6_3/m$. The top and bottom sets of symbols, ticks (marking the positions of Bragg reflections), and difference curves are for the $P\bar{6}2m$ and $P6_3/m$ models, respectively. The residuals Rwp and Rp, whose definitions are given in the GSAS manual (11), are calculated only for the Bragg contribution to the diffraction patterns. Bragg reflections due to the solid $R\bar{3}c$ phase of nitrogen (13) are subtracted.

$P6_3/m$ gagarinite (21) and Zachariasen's $P\bar{6}2m$ (25) structures (Tables 5 and 6, respectively). In the first, the coordination polyhedra around the ($\frac{3}{4}Y^{3+}$, $\frac{1}{4}Na^+$) position are tricapped trigonal prisms (site $2d$), while the remaining sodium ions are split between partially occupied positions with tricapped trigonal prism and trigonal antiprism coordinations (two sites $4e$), as inferred from the single crystal data. To avoid any ambiguities and artifacts associated with refinement of the split occupancies at the two $4e$ positions, related to a strong background and broadened reflections,

we modified this structural model by placing all the remaining sodium atoms at one site that has the trigonal antiprismatic coordination, i.e., $\frac{1}{4}Na^+$ at $4e$ (Table 5). This site, in fact, corresponds to the partially occupied octahedral $2h$ position in the $P\bar{6}$ structure. The starting positional parameters for the atoms in the $P\bar{6}2m$ structure were those for $K_{1.5}Ce_{1.5}F_6$ (25). From the results of the Rietveld refinements (Fig. 4), it is not possible to precisely indicate a preferable structural model for $Na_{1.5}Y_{1.5}F_6$ above 20 GPa, apart from the fact that the two hexagonal space groups have different extinction rules and the 001 reflection is no longer present or too weak to be observed ($l = 2n$ in $P6_3/m$). Like in the case of space group $P\bar{6}$ (Tables 1 and 3), some distances between fluorine atoms and sodium atoms at the

TABLE 1

Structural Data Obtained from a Full Rietveld Refinement of the Pattern Collected at 1.5 GP—$P\bar{6}(Z = 1)$, $a = 5.9148(1)$ Å, $c = 3.4960(1)$ Å, $V = 106.145(5)$ Å³

Atom	Site	x	y	z	Frac.
Y(1)	$1a$	0	0	0	1
Y(2)	$1f$	$\frac{2}{3}$	$\frac{1}{3}$	$\frac{1}{2}$	$\frac{1}{2}$
Na(1)	$1f$	$\frac{2}{3}$	$\frac{1}{3}$	$\frac{1}{2}$	$\frac{1}{2}$
Na(2)	$2h$	$\frac{1}{3}$	$\frac{2}{3}$	0.689(5)	$\frac{1}{2}$
F(1)	$3j$	0.646(1)	0.1256(8)	0	1
F(2)	$3k$	0.697(1)	0.722(1)	$\frac{1}{2}$	1

Selected distances (Å)			
Y(1)	−F(1)	$(3 \times)$	2.548(7)
	−F(2)	$(6 \times)$	2.453(3)
[Y(2), Na(1)]	−F(1)	$(6 \times)$	2.105(3)
	−F(2)	$(3 \times)$	2.216(7)
Na(2)	−F(1)	$(3 \times)$	2.636(8)
	−F(2)	$(3 \times)$	2.116(7)

Note. Estimated standard deviations are given in brackets.

TABLE 2

Structural Data Obtained from a Full Rietveld Refinement of the Pattern Collected at 1.5 GPa—$P\bar{6}2m$ ($Z = 1$), $a = 5.9148(1)$ Å, $c = 3.4960(2)$ Å, $V = 106.145(6)$ Å³

Atom	Site	x	y	z	Frac.
Na	$2d$	$\frac{1}{3}$	$\frac{2}{3}$	$\frac{1}{2}$	$\frac{3}{4}$
Y(1)	$2d$	$\frac{1}{3}$	$\frac{2}{3}$	$\frac{1}{2}$	$\frac{1}{2}$
Y(2)	$1a$	0	0	0	1
F(1)	$3f$	0.618(1)	0	0	1
F(2)	$3g$	0.223(1)	0	$\frac{1}{2}$	1

Selected distances (Å)			
[Na,Y(1)]	−F(1)	$(6 \times)$	2.542(2)
	−F(2)	$(3 \times)$	2.367(4)
Y(2)	−F(1)	$(3 \times)$	2.257(7)
	−F(2)	$(6 \times)$	2.190(3)

Note. Estimated standard deviations are given in brackets.

TABLE 3

Structural Data Obtained from a Full Rietveld Refinement of the Pattern Collected at 19.9 GPa—$P\bar{6}(Z = 1)$, $a = 5.6128(1)$ Å, $c = 3.3366(2)$ Å, $V = 91.60(1)$ Å³

Atom	Site	x	y	z	Frac.
Y(1)	$1a$	0	0	0	1
Y(2)	$1f$	$\frac{2}{3}$	$\frac{1}{3}$	$\frac{1}{2}$	$\frac{1}{2}$
Na(1)	$1f$	$\frac{2}{3}$	$\frac{1}{3}$	$\frac{1}{2}$	$\frac{1}{2}$
Na(2)	$2h$	$\frac{1}{3}$	$\frac{2}{3}$	0.620(2)	$\frac{1}{2}$
F(1)	$3j$	0.613(1)	0.076(1)	0	1
F(2)	$3k$	0.687(1)	0.738(1)	$\frac{1}{2}$	1

Selected distances (Å)			
Y(1)	−F(1)	$(3 \times)$	2.415(8)
	−F(2)	$(6 \times)$	2.334(3)
[Y(2), Na(1)]	−F(1)	$(6 \times)$	2.126(5)
	−F(2)	$(3 \times)$	2.216(7)
Na(2)	−F(1)	$(3 \times)$	2.398(6)
	−F(2)	$(3 \times)$	1.863(6)

Note. Estimated standard deviations are given in brackets.

TABLE 4

Structural Data Obtained from a Full Rietveld Refinement of the Pattern collected at 19.9 GPa—$P\bar{6}2m$ ($Z=1$), $a = 5.6142(2)$ Å, $c = 3.3367(2)$ Å, $V = 91.62(1)$ Å^3

Atom	Site	x	y	z	Frac.
Na	2d	$\frac{1}{3}$	$\frac{2}{3}$	$\frac{1}{2}$	$\frac{3}{4}$
Y(1)	2d	$\frac{1}{3}$	$\frac{2}{3}$	$\frac{1}{2}$	$\frac{1}{4}$
Y(2)	1a	0	0	0	1
F(1)	3f	0.558(2)	0	0	1
F(2)	3g	0.2599(8)	0	$\frac{1}{2}$	1

Selected distances (Å)

[Na, Y(1)]	$-F(1)$	$(6\times)$	2.348(1)
	$-F(2)$	$(3\times)$	2.108(3)
Y(2)	$-F(1)$	$(3\times)$	2.482(8)
	$-F(2)$	$(6\times)$	2.216(3)

Note. Estimated standard deviations are given in brackets.

TABLE 6

Structural Data Obtained from a Full Rietveld Refinement of the Pattern Collected at 21.1 GPa—$P\bar{6}2m$ ($Z=1$), $a = 5.6018(2)$ Å, $c = 3.3291(2)$ Å, $V = 90.47(1)$ Å^3

Atom	Site	x	y	z	Frac.
Na	2d	$\frac{1}{3}$	$\frac{2}{3}$	$\frac{1}{2}$	$\frac{3}{4}$
Y(1)	2d	$\frac{1}{3}$	$\frac{2}{3}$	$\frac{1}{2}$	$\frac{1}{4}$
Y(2)	1a	0	0	0	1
F(1)	3f	0.5806(9)	0	0	1
F(2)	3g	0.2815(8)	0	$\frac{1}{2}$	1

Selected distances (Å)

[Na, Y(1)]	$-F(1)$	$(6\times)$	2.364(1)
	$-F(2)$	$(3\times)$	2.028(3)
Y(2)	$-F(1)$	$(3\times)$	2.349(5)
	$-F(2)$	$(6\times)$	2.293(3)

Note. Estimated standard deviations are given in brackets.

partially occupied $4e$ site are shorter than 2.0 Å (Table 5). It should be pointed out that already at ambient pressures without any pressure effects on the bonding and lattice parameters (see below), the distances between the fluorine and sodium cations at the partially occupied sites in the $P\bar{6}$ and $P6_3/m$ gagarinite structures are short (3, 20). On the other hand, none of the distances between the cations and anions in the $P\bar{6}2m$ structure of the β-Na$_2$ThF$_6$ type, with no partially occupied sites, is anomalously short at high pressures (Tables 2, 4, and 6).

The pressure dependence of lattice parameters and unit-cell volumes, obtained with a Le Bail method for space group $P\bar{6}2m$ using the program PowderCell (27), is shown in Fig. 5. The unit-cell volume for the powder pattern collected at ambient pressure is 108.99(4) Å^3. The same Birch–Murnaghan equation of state (EoS) can be used for the

entire compression curve up to 22.2 GPa. It is represented by the zero-pressure bulk modulus $K_0 = 79 \pm 2$ GPa, the first pressure derivative of the bulk modulus $K' = 4.92 \pm 0.20$, and the unit-cell volume at ambient pressure $V_0 = 109.1 \pm 0.1$ Å^3. When the K' parameter is equal to 4, the compression curve is represented by $K_0 = 87 \pm 1$ GPa and $V_0 = 108.8 \pm 0.1$ Å^3. This demonstrates that there is no volume change associated with all these reversible transformations. The lattice parameters and unit-cell volumes obtained with the same method for space groups $P\bar{6}$ and $P6_3/m$ are practically identical (compare the lattice parameters and unit cell volumes in Tables 1–6) and do not change the EoS parameters within their estimated standard deviations.

CONCLUSIONS

The results of this study show that hexagonal Na$_{1.5}$Y$_{1.5}$F$_6$ does not undergo any major phase transition up to about 22 GPa. At near ambient pressures, the structure is of the Na$_{1.5}$Nd$_{1.5}$F$_6$ type ($P\bar{6}$, $Z=1$), found in other low-temperature sodium lanthanide fluorides (2, 3, 20, 22). In this structure, the cations are distributed at two Y^{3+} and ($\frac{1}{2}$Na$^+$, $\frac{1}{2}$Y^{3+}) trigonal prismatic and one $\frac{1}{2}$Na$^+$ octahedral sites. As inferred from full profile Rietveld refinements of diagrams collected at higher pressures, pressure-induced order−disorder phenomena lead to the formation of the gagarinite-type structure ($P6_3/m$, $Z=1$) above 20 GPa with only two available cationic sites (21)—the ($\frac{3}{4}$Y^{3+}, $\frac{1}{4}$Na$^+$) trigonal prism and $\frac{1}{4}$Na$^+$ trigonal antiprism positions. Alternatively, the pressure-induced order−disorder phenomena could involve the phase of the β-Na$_2$ThF$_6$ type with $P\bar{6}2m$ ($Z=1$) symmetry with two nine-fold coordinated cationic sites, originally proposed for K$_{1.5}$La$_{1.5}$F$_6$, K$_{1.5}$Ce$_{1.5}$F$_6$, and Na$_{1.5}$Y$_{1.5}$F$_6$ at low temperatures (14, 25).

TABLE 5

Structural Data Obtained from a Full Rietveld Refinement of the Pattern Collected at 21.1 GPa—$P6_3/m$ ($Z=1$), $a = 5.6022(2)$ Å, $c = 3.3295(2)$ Å, $V = 90.50(1)$ Å^3

Atom	Site	x	y	z	Frac.
Y	2d	$\frac{2}{3}$	$\frac{1}{3}$	$\frac{1}{4}$	$\frac{3}{4}$
Na(1)	2d	$\frac{2}{3}$	$\frac{1}{3}$	$\frac{1}{4}$	$\frac{1}{4}$
Na(2)	4e	0	0	0.646(4)	$\frac{1}{4}$
F	6h	0.2814(5)	0.3563(6)	$\frac{1}{4}$	1

Selected distances (Å)

[Y, Na(1)]	$-F$	$(3\times)$	2.227(4)
		$(6\times)$	2.317(2)
Na(2)	$-F$	$(3\times)$	1.855(4)
		$(3\times)$	2.250(8)
		$(3\times)$	2.714(11)

Note. Estimated standard deviations are given in brackets.
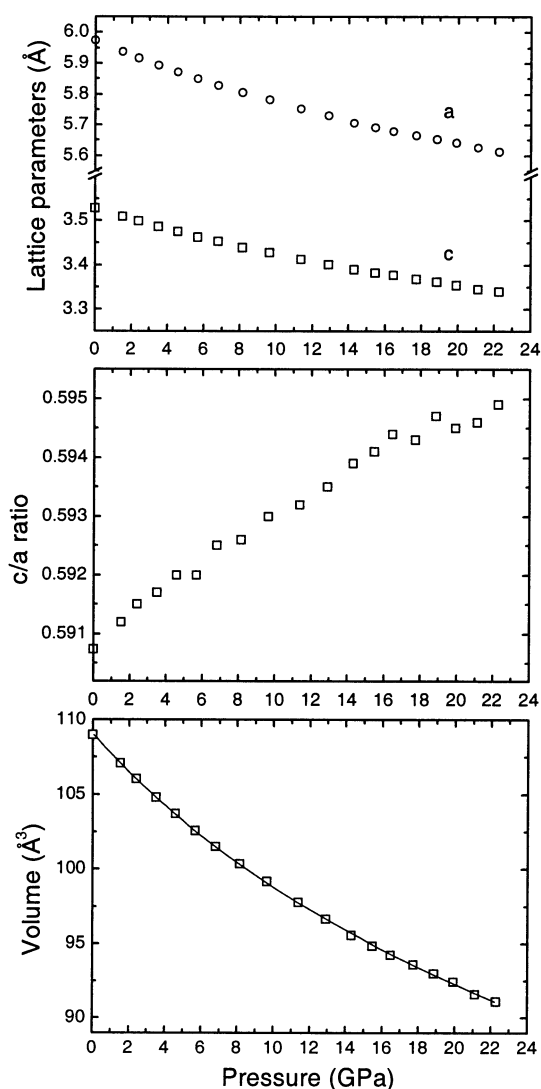
FIG. 5. Pressure evolution of axial lattice parameters and of unit-cell volumes. The line represents the Birch–Murnaghan equation of state: $K_0 = 79 \pm 2$ GPa, $K' = 4.92 \pm 0.20$, $V_0 = 109.1 \pm 0.1$ Å^3.

There is no volume change associated with all these reversible processes.

The high-temperature forms of sodium lanthanide fluorides and sodium yttrium fluoride have the fluorite structure at atmospheric conditions ($Fm\bar{3}m$, $Z = 4$) (14–18, 21). The $P\bar{6} \rightarrow Fm\bar{3}m$ or $P6_3/m \rightarrow Fm\bar{3}m$ high-temperature phase transitions of the order–disorder type result in a random distribution of all the cations over one crystallographic position in the cubic crystal lattice. Future investigations on

luminescence, that is a precise probe for site symmetry, would shed more light on whether there is a common mechanism for the changes in cationic distribution in this and other $Na_{1.5}Ln_{1.5}F_6$ ($Ln = $ La–Tm) compounds at different pressure and temperature conditions.

REFERENCES

1. R. Burkhalter, I. Dohnke, and J. Hulliger, *Prog. Cryst. Growth Charact.* **42,** 1 (2001).
2. N. Martin, P. Boutinaud, M. Malinowski, R. Mahiou, and J. C. Cousseins, *J. Alloys Compd.* **275–277,** 304 (1998).
3. D. Zakaria, R. Mahiou, D. Avignant, and M. Zahir, *J. Alloys Compd.* **257,** 65 (1997).
4. P. Blanchfield and G. A. Saunders, *J. Phys. C: Solid State Phys.* **12,** 1979 (4673); P. Blanchfield, G. A. Saunders, and T. Hailing, *J. Phys. C: Solid State Phys.* **15,** 2081 (1982); S. Salaün, M. T. Fornoni, A. Bulou, M. Rousseau, P. Simon, and J. Y. Gesland, *J. Phys.: Condens. Matter* **9,** 6941 (1997); S. Salaün, A. Bulou, M. Rousseau, B. Hennion, and J. Y. Gesland, *J. Phys. Condens. Matter* **9,** 6957 (1997); A. Sen, S. L. Chaplot, and R. Mittal, *Phys. Rev. B* **64,** 024304 (2001).
5. E. Sarantopoulou, Y. S. Raptis, E. Zouboulis, and C. Raptis, *Phys. Rev. B* **59,** 4154 (1999).
6. L. Shenxin, C. Yuanbin, Z. Xuyi, and W. Lizhong, J. *Alloys Compd.* **255,** 1 (1997).
7. A. Grzechnik, K. Syassen, I. Loa, M. Hanfland, and J.-Y. Gesland, *Phys. Rev. B* **65,** 104102.
8. A. Boultif and D. Löuer, *J. Appl. Cryst.* **24,** 987 (1991).
9. A. P. Hammersley, S. O. Svensson, M. Hanfland, A. N. Fitch, and D. Häusermann, *High Pressure Res.* **14,** 235 (1996).
10. H. K. Mao, J. Xu, and P. M. Bell, *J. Geophys. Res.* **91,** 4673 (1986).
11. A. C. Larson and R. B. von Dreele, GSAS: "General Structure Analysis System," Los Alamos National Laboratory, 2000.
12. P. W. Stephens, *J. Appl. Cryst.* **32,** 281 (1999).
13. M. Hanfland, M. Lorenzen. C. Wassilew-Reul, and F. Zontone, *Rev. High Pressure Sci. Technol.* **7,** 787 (1998).
14. D. M. Roy and R. Roy, *J. Electrochem. Soc.* **111,** 421 (1964).
15. F. Hund, *Z. Anorg. Allge. Chem.* **261,** 106 (1950).
16. K. Narasimha Reddy, M. A. H. Shareef, and N. Pandaraiah, *J. Mater. Sci. Lett.* **2,** 83 (1983).
17. W. H. Zachariasen, *Acta Crystallogr.* **2,** 388 (1949).
18. Y. Le Fur, N. M. Khaidukov, and S. Aléonard, *Acta Crystallogr. C* **48,** 978 (1992).
19. G. Brunton, *Acta Crystallogr.* **25,** 600 (1969).
20. J. H. Burns, *Inorg. Chem.* **4,** 881 (1965).
21. O. V. Frank-Kamenetskaya, V. S. Fundamenskii, A. K. Tsytsenko, and V. A. Frank-Kamenetskii, *Crystal. Rep.* **39,** 923 (1994).
22. H. S. Kiliaan, J. F. A. K. Kotte, and G. Blasse, *Chem. Phys. Lett.* **133,** 425 (1987); D. Zakaria, M. T. Fournier, R. Mahiou, and J. C. Cousseins, *J. Alloys Compd.* **188,** 250 (1992).
23. G. Brunton, *Acta Crystallogr. B* **25,** 600 (1969).
24. A. Dib, M. T. Roux, and S. Aléonard, *J. Solid State Chem.* **66,** 47 (1987).
25. W. H. Zachariasen, *Acta Crystallogr.* **1,** 265 (1948).
26. G. Brunton, *Acta Crystallogr. B* **25,** 2163 (1969).
27. W. Kraus and G. Nolze, "CPD Newsletter no. 20." International Union of Crystallography, 1998.